Revisiting long-range dependence in annual precipitation

[1*]Theano Iliopoulou, [1]Simon Michael Papalexiou, [1]Yannis Markonis and [1]Demetris Koutsoyiannis

[1]Department of Water Resources, Faculty of Civil Engineering, National Technical University of Athens, Heroon Polytechneiou 5, GR-157 80 Zographou, Greece

* Corresponding author. Tel.: +30 6978580613

E-mail address: anyily@central.ntua.gr

Abstract

Long-range dependence (LRD), the so-called Hurst-Kolmogorov behaviour, is considered to be an intrinsic characteristic of most natural processes. This behaviour manifests itself by the prevalence of slowly decaying autocorrelation function and questions the Markov assumption, often habitually employed in time series analysis. Herein, we investigate the dependence structure of annual rainfall using a large set, comprising more than a thousand stations worldwide of length 100 years or more, as well as a smaller number of paleoclimatic reconstructions covering the last 12,000 years. Our findings suggest weak long-term persistence for instrumental data (average H = 0.59), which becomes stronger with scale, i.e. in the paleoclimatic reconstructions (average H = 0.75).

Keywords: Long-range dependence, Hurst behaviour, long-term persistence, rainfall variability, precipitation reconstructions, proxy records

1. Introduction

Since Hurst [1951] brought long-term persistence, also known as long-range dependence (LRD), into scientific discourse, the interest in this time-series behaviour has been rising. This is mainly due to its serious implications into the modelling and design processes in various scientific fields and particularly in water resources [*O'Connell et al.*, 2015]. Another fact significantly contributing to its growing popularity is that LRD has been identified in many climatic variables, such as temperature [*Pelletier*, 1998; *Koutsoyiannis*, 2003], rainfall [*Fraedrich and Larnder*, 1993; *Pelletier and Turcotte*, 1997], wind power [*Haslett and Raftery*, 1989] and the North-Atlantic oscillation index [*Stephenson et al.*, 2000]. Hurst behaviour also has a strong physical basis, as it is derived from the principle of entropy maximization [*Koutsoyiannis*, 2011a], a principle which can be used to determine the theoretical probability distribution model for rainfall [*Papalexiou and Koutsoyiannis*, 2012]. More detailed discussion on the history and relevance of the Hurst behaviour can be found in the recent review paper by O'Connell et al. [2016].

In this analysis, we aim to investigate the dependence properties of annual rainfall. Studies regarding LRD in annual rainfall are usually limited to a specific area and/or utilize datasets of relatively short lengths [*Kantelhardt et al.*, 2006; *Bunde et al.*, 2013; *Zhai et al.*, 2014]. Short record lengths can introduce bias into the estimation of long-term persistence properties, which in general, need more than 100 years in order to avoid underestimation (and, in cases of very strong dependence, even more than 1000) [*Koutsoyiannis and Montanari*, 2007]. A majority of other studies investigate the dependence structure of rainfall at sub-annual or even smaller scales [*Papalexiou et al.*, 2011], but in that case, the phenomenon gets complicated due to the combined effects of seasonal variation and intermittency. On the other hand, paleoclimatic reconstructions suggest strong LRD behaviour in multi-decadal to centennial time scales [*Pelletier and Turcotte*, 1997; *Markonis and Koutsoyiannis*, 2016]. Evidently, there are still ample grounds for research on the existence of LRD in annual precipitation.

Herein, we have analyzed more than one thousand annual precipitation records of length of a hundred years or more from different areas of the world, as well as approximately 70 paleoclimatic records spanning the time from 12 thousand years ago until the present day. To quantify LRD, we estimated the Hurst coefficient, by applying two algorithmic versions of the aggregated variance method and employed Monte Carlo method to identify a common Hurst coefficient for all the records. Additionally, we performed a simple test on the autocorrelation structure of the first few lags to examine whether the hypothesis of a Markovian autocorrelation structure is justified or not. Finally, we investigated the effect of time-scale and record length on LRD estimation using the paleoclimatic series.

2. Dataset

The instrumental data were obtained from the Global Historical Climatology Network (GHCN-Daily, http://www.ncdc.noaa.gov/oa/climate/ghcn-daily/), which contains daily data from more than 50 000 land surface stations around the globe. A significant percentage of these records exhibit the typical issues of most datasets available, i.e. missing values, short record length and rainfall values of questionable quality, such as unrealistic outliers. In order to restrict data quality to a significantly high level, we filtered the dataset using certain criteria.

Initially, we chose to study only the stations satisfying the following conditions: (a) record length over 100 years, (b) missing daily values percentage less than 20% of the record length and, (c) suspect values with quality flags less than 0.1%. This first quality screening resulted in 3477 stations of daily data with lengths varying from 100 years to 173 years. Then, in order to construct the annual series we first deleted all daily values assigned quality flags, indicating unrealistically large values, and then estimated the average daily value per year. Notably, because of the existence of missing values within some records, summing up daily values to obtain the annual total would result in smaller estimates than the real ones. Instead, it is more robust to estimate the daily mean values per year as the mean value estimate can be accurate even in the presence of some missing values. This is equivalent to estimating the annual total by first infilling the daily missing values of a year with the daily average of the year. Years having more than 20 missing daily values were considered missing and their annual estimate was not derived. Via the abovementioned method, the 3477 daily stations are aggregated to the annual timestep. Among these stations, there are different combinations of record lengths and number of missing yearly values, e.g., 558 stations having 100 years in a sequence with no missing values, 1474 stations with more than 100 annual values and only eight stations without any missing values. We choose to analyze 1265 stations having more than 100 annual values and a missing yearly values percentage less than 15%. Obviously, this choice ensures a higher quality dataset for our analysis on the annual time step.

Paleoclimatic data can also be used to determine the existence of LRD in climatic variables since they cover quite larger scales compared to the instrumental data sets [*Mandelbrot and Wallis*, 1969; *Koutsoyiannis*, 2003; *Bunde et al.*, 2013; *Markonis and Koutsoyiannis*, 2013]. Herein, we used 68 paleoclimatic records of rainfall reconstructions located mainly in the northern hemisphere to explore time scales reaching up to 12,000 years. Three different data sets were used corresponding to the proxy variable used for the reconstruction process; i.e. tree rings, speleothems and '*other*' (including lake sediments, pollen, corals and multi-proxy reconstructions). The 40 time series of tree ring reconstructions are the largest data set and have a mean sample size of 900 values at an annual time scale (see Table 1). The other two data sets, with 16 and 12 time series correspondingly, in most cases have fewer values and varying time resolutions, ranging between 1 and 100 years. It must be noted that the speleothem records are proxy records of $\delta^{18}O$, a variable which is linearly linked to rainfall.

3. Analysis and results

3.1 Aggregated variance method

The method employed herein is based on the study of the variability of the data averaged at different timescales. The method is typically referred to as aggregated variance method, but what it actually aggregates is the timescale and not the variance. Specifically, let X_j be a stationary process in discrete time *j* (referring to years in our case) with standard deviation σ and let

$$X_j^{(k)} = \frac{1}{k} \sum_{l=(j-1)k+1}^{jk} X_l, k = 1, 2, 3... \tag{1}$$

denote the averaged process at timescale *k*, with standard deviation $\sigma^{(k)}$. In the case of an uncorrelated process, the standard deviation of $X_j^{(k)}$ is obtained by $\sigma^{(k)} = \sigma / \sqrt{k}$. In other cases, e.g. if the process is Fractional Gaussian Noise (or a Hurst-Kolmogorov process) the abovementioned law is invalid. Instead one obtains the elementary scaling property:

$$\sigma^{(k)} = k^{H-1}\sigma \tag{2}$$

where *H* is the Hurst coefficient, which for stationary and positively correlated processes varies in the range (0.5, 1) [*Beran*, 1994]. The value of *H* = 0.5 denotes time independence, while smaller values are indicative of anti-persistence. The autocorrelation of the aggregated process is independent of the scale of aggregation *k* and is given as follows:

$$\rho_j^{(k)} = \rho_j = \frac{1}{2}\left[\left(j+1\right)^{2H} + \left(j-1\right)^{2H}\right] - j^{2H} \qquad j > 0 \tag{3}$$

To apply the method to the data we used a graphic tool, the climacogram [*Koutsoyiannis*, 2011b], which is the double-logarithmic plot of the standard deviation $\sigma^{(k)}$ of the aggregated time series at scale k versus the time scale k. The H value is estimated as the slope of the fitted line (least squares regression). In a variant of that method, the estimation bias of the standard deviation, which depends on the time-scale of aggregation, is also considered (see 3.2 below).

Each averaged time series is constructed as follows. For every scale k, the data are divided into n groups, the number of which is obtained as the fraction of the data length L versus the scale value k. For example in time scale k = 4, 120 years would be divided in 30 non-overlapping groups of 4 years. Subsequently, the values within each group are averaged according to equation 1. However, when missing values are encountered, the process of averaging may become problematic depending on the number of missing values; if more than a half of the values is missing, then the estimate would be quite uncertain [*Markonis*, 2015]. To overcome the issue, we use a simple criterion on the number of missing values before estimating the averaged series within each group: (a) for scale k = 2 the average value is estimated only when both values exist (b) for scales $k \geq 3$ the average value is estimated only when there are at least three values within the group. According to the latter rule, we estimated the averaged series for all the scales between $k_{\min}$ and $k_{\max}$, where $k_{\min} = 1$ and $k_{\max} \leq L/10$ so that the variance in the maximum scale is estimated from at least 10 values [*Koutsoyiannis*, 2003]. For a 100-year record length this would be the variance of the decadal means.

The results of the algorithm implementation for the instrumental data are shown in Table 2 and Figure **Figure** 1, suggesting some evidence of weak long range dependence. More specifically, it was found that 85% of the data exhibit $H \geq 0.5$, yet with notable variation. For example, only half of the data show $H \geq 0.59$, i.e. a more pronounced dependence structure. A very strong dependence structure, $H \geq 0.80$ is reported for 2.5% of the records, while for 15% of them we observe lack of dependence. For the 95% confidence interval, H values fluctuate between 0.4 and 0.8. In paleoclimatic data, the Hurst coefficient shows a tendency for higher estimates, as well as an increased range of values (Figure 2).

In order to test the effects of our parametric choices for the value of the minimum and maximum scale, we examined how the median and the variance of H estimates vary for different $k_{\min}$ and $k_{\max}$. As can be seen in Figure 3, the variance of the Hurst parameter estimate becomes larger as the value of the minimum scale $k_{\min}$ increases; yet the value of the median in the estimate remains the same. Therefore, our choice of $k_{\min} = 1$ is well-justified, since greater values of $k_{\min}$ only amplify the uncertainty in H estimation. In addition, the observation of the same median strengthens our hypothesis of the LRD structure, because in the alternative hypothesis of short term dependence, we would notice some change in the climacogram curvature and correspondingly to the logarithmic slope. The results for the $k_{\max}$ were similar. It can be seen in Figure 4 that the decrease in the number of values in the last scale increases the variance of the Hurst parameter estimate in this case too. Therefore, the choice of $n \geq 10$ leads to more reliable results compared to using smaller values of n.

3.2 Least Squares Based on Standard Deviation Method (LSSD)

Koutsoyiannis [2003] demonstrated how the use of the classical estimator for the standard deviation can introduce significant negative bias in the estimation of the Hurst parameter by the aggregated variance method. This is because the hypothesis of independence, which is a necessary condition for the use of the estimator, is violated in the case of processes with strong LRD behaviour. This shortcoming may be overcome by the use of the Least Squares Based on Standard Deviation Method (LSSD) [*Koutsoyiannis*, 2003; *Tyralis and Koutsoyiannis*, 2011], which performs a simultaneous estimation of the Hurst parameter H and the standard deviation σ using an approximately unbiased estimator for the latter.

Here, for simplicity reasons we applied the LSSD method [*Tyralis and Koutsoyiannis*, 2011] only to the sample of the 558 (44% of the total) stations with no missing values and then, compared our estimate with the one obtained by the aggregated variance method for the same sample. As shown in Table 3 and Figure 5 the two methods show small deviations from each other. Overall, the value of the bias fluctuates between 1-2% with the bias in the estimate of the average being approximately 1%. The bias is negligible in this case because the estimated Hurst parameter is not very high.

3.3 Monte Carlo Testing

We also investigated the assumption that the observed distribution of the sample estimates of H results from a single model with a specific true value (sometimes referred to as population value) of the Hurst coefficient. In order to produce a theoretical sample of time series exhibiting Hurst dynamics, we used a simple algorithm that generates Fractional Gaussian Noise based on a multiple timescale fluctuation approach [*Koutsoyiannis*, 2002]. We generated 1265 time series from a Gaussian distribution that reproduce the record length, the mean and the standard deviation of the empirical sample, repeated the same procedure for several theoretical H values and then estimated the empirical ones. We should note that there may be some cases where moderate departures from normality are observed for the annual rainfall distribution, especially in arid/semi-arid regions of the world or regions severely affected by the El Nino-Southern Oscillation (ENSO). Still the use of the assumption of normality for the synthetic records, albeit simplifying, is justifiable as for the majority of the stations the Central Limit Theorem holds (therefore normality is a good approximation) while in general, using Monte Carlo experiments, we were able to find that the estimation of the Hurst coefficient is practically insensitive to the underlying distribution. Subsequently, the distribution of the empirical estimates for the synthetic time series was compared to the distribution of the empirical estimates for the historic time series used in the analysis. It appears that the value of $H = 0.58$ (Figure 6) yields the most satisfactory match. However, it is worth noticing that that 2.5% of the stations, exhibiting $H > 0.8$, are outside the range of the theoretical distribution.

3.4 Autocorrelation analysis

The estimated Hurst coefficient is not high enough to allow for any certain conclusion on the type of the dependence structure, since relatively low Hurst coefficients (0.5-0.6) can be estimated when there is short range dependence or no dependence at all due to algorithmic inadequacies, sample bias and estimation uncertainty. To this end, we have employed the autocorrelation function, to further examine the dependence properties of rainfall. Still one should keep in mind that the classical autocorrelation estimator, as in the case of standard deviation, is biased downwards [*Koutsoyiannis*, 2003; *Dimitriadis and Koutsoyiannis*, 2015]. However, since the estimator is biased downwards, any result in favour of LTP, would mean that in reality, the LTP is even stronger.

The autocorrelation coefficients of the first three lags for the instrumental data are low (Table 4). On further investigation, we tested whether independence is a plausible scenario for the dependence structure of our data. We produced 1265 independent, i.e. uncorrelated, time series of the same sample size and estimated the sample autocorrelation coefficients (Figure 7). It can be seen that for all three lags the value of the median of the historic data is greater than the one estimated from uncorrelated synthetic data. This is more obvious in the case of autocorrelation of lag-1 where for confidence interval 95% the values of the independent data fluctuate in the range –0.175 to 0.173, while the historic ones are in the range –0.09 to 0.37. In addition, in all three cases, the historic samples exhibit significantly fewer negative values than the uncorrelated ones.

The above results could be typical for a Markov process too, also known as AR(1) process. To address this issue, a simple ad hoc test, which exploits the distinctive properties of Markov processes, was designed. Under the Markov hypothesis, the theoretical autocorrelation coefficient for lag 2 would be estimated as $\rho_2 = \rho_1^2$, where ρ_1 is the known empirical autocorrelation. Likewise, the Markovian autocorrelation coefficient for lag 3 would be given as $\rho_3 = \rho_1^3$. The resulting theoretical estimate is compared to the empirical one for the same lag; if the empirical value is higher than the theoretical AR(1) one, then the Markov hypothesis weakens.

We applied this comparison to the 52% of the stations for which all the autocorrelation coefficients for lags 1-3 are positive (Figure 8). It is evident that the empirical estimates are considerably higher than the theoretical ones resulting from an AR(1) structure and therefore, the Markov assumption becomes less likely. In addition, the empirical estimates do not follow the exponential convergence to zero of the Markovian ones, but instead, remain approximately stable for lags 2 and 3; this is in agreement with the theoretical behaviour of LRD whose distinctive feature is the existence of slowly decaying autocorrelation function [*Beran*, 1994].

Having tested the cases of independence and short-range dependence, we finally examined whether the autocorrelation structure is consistent with that of a FGN model via a visual comparison of the two. In Figure 9 the empirical autocorrelation coefficient ρ_1 is plotted against the corresponding empirical Hurst coefficient *H* as obtained from Equation (2). The theoretical autocorrelation values of a FGN model as obtained from Equation (3) are plotted as well. The diagram shows that the autocorrelation structure is consistent with that of a FGN model. The deviation between the theoretical and the empirical estimates becomes greater in the region of high values of *H*; still this is justified due to the increased negative bias in the autocorrelation estimation in that case.

3.5 Paleoclimatic Data

Paleoclimatic data reveal a stronger form of dependence at larger time scales, which is in good agreement with other relevant studies [*Bunde et al.*, 2013; *Franke et al.*, 2013]. In general, we can divide proxy data into three categories based on their temporal resolution; high resolution data with annual time step (mainly tree-rings), medium resolution data with decadal time step (mainly speleothems) and low resolution data with centennial time increments (such as lake sediments or pollen). However, certain factors should be taken in consideration regarding some fundamental uncertainties about rainfall reconstruction from proxy variables. Often, tree-rings represent areal reconstructions of precipitation and in some cases the area covered is rather large, e.g. CE11 (as defined in Table 1). Since the individual time series are cross-correlated, their aggregation to a single time series might increase *H* [Granger, 1980]. To address this issue a random cross-examination of individual tree-rings records was performed and it was confirmed that the individual series exhibit the same behaviour as the aggregated records. In addition, until recently, the most common approach to transform the proxy variable (tree-ring width) to the reconstructed one (rainfall) was through a method that involved detrending and/or pre-whitening of the original time series. This methodology has a severe impact on the low-frequency variability [*Briffa et al.*, 1996; *Helama et al.*, 2004], and thus on *H* estimation, as presented in Figure 2 (red diagonal lines). Detrended/pre-whitened time series have a mean *H* equal to 0.5; while the rest of the records which are derived using the Regional Curve Standardization [*Briffa et al.*, 1992] or the Neural Networks [*Ni et al.*, 2002] methods have a mean near 0.72.

On the other hand, in some cases such as the time series with centennial time resolution, the uncertainties in the correct estimation of the precipitation amount are so high that the record is strongly smoothed in order to depict only major shifts of the mean. These data sets (e.g. As05 or CC09 as defined in Table 1) are of small sample sizes and thus H estimates are unavoidably pushed towards values that reach close to 1 (Figure 2; green diagonal lines). Even in larger data sets, i.e. speleothems, if the smoothing happens to be combined with a strong monotonic trend of the original data then again H values would falsely tend towards 1 (Figure 2; orange diagonal lines). Such estimates cannot be included in the estimation of H, which finally reaches 0.75 for the paleoclimatic data. However, they cannot be totally neglected as they provide some qualitative evidence for the long term change in rainfall, which includes both long term trends and abrupt shifts in the mean.

The effect of record length on LRD is further explored by partitioning the reconstructed records to smaller segments, which can be achieved by estimating H through a moving time window of variable length (i.e. 50, 100, 250 and 500 years). Since the tree-rings have annual resolution, they are suitable for such analysis, as the results are directly comparable with the estimates of the instrumental time series. To limit any methodological uncertainties, the CL02 dataset was used, which contains 15 records with average H ($\overline{H}$) equal to 0.75, has record length close to 1000 years and is not detrended or pre-whitened. The results show that if the sample size is equal to the instrumental records (100 years) then LRD structure fluctuates between white noise (H = 0.5) and strong Hurst behaviour (H = 0.9), with $\overline{H}$ = 0.71 (Figure 10). As the record length increases, H values are constrained to (0.7, 0.8) and $\overline{H}$ converges to 0.75. The results are reproduced for an equal number of synthetic time series with similar size and LRD properties. However, the even higher values of Hurst coefficient (H > 0.8) found in other paleoclimatic reconstructions (Figure 2) cannot be simply attributed to sample size bias (their behaviour cannot be reproduced by synthetic time series). This suggests that either rainfall presents different dependence structures in sub-decadal and above-decadal scales [*Markonis and Koutsoyiannis*, 2016], or that the stronger LRD is artificial, introduced to the precipitation reconstructions through some intrinsic properties of the proxy variables (e.g., karst transit time in speleothems [*Dee et al.*, 2015]).

4. Discussion and conclusions

The analysis of the global instrumental data set shows that there are notable indications of weak LRD in the annual rainfall. As the Hurst parameter is not very high, the aggregated variance method induces only 1-2% negative bias in the Hurst coefficient estimation and therefore, the best population value of H that has been shown through Monte Carlo estimation to account for the observed sampling variability, H = 0.58, may be considered accurately representative for instrumental data.

The study of the autocorrelation function shows that it is consistent with the autocorrelation of a FGN model, even though for a certain percentage of the stations the Markov hypothesis could not be falsified. Specifically, the existence of negative correlations in all three lags examined did not permit the application of the abovementioned method in the case of the 48% of the stations. Some studies using smaller data sets [*Potter*, 1979; *Fraedrich and Blender*, 2003; *Kantelhardt et al.*, 2006] supported the appropriateness of the Markov structure, but they did not investigate the differences between actual and theoretical auto-correlation in larger lags (Figure 8). These differences might be quite small, and thus allow the stochastic modelling of annual rainfall as a Markovian process for record lengths below 100 years. It has been shown though, that they might have serious implications when it comes to the estimation of trend significance and as a result, the observed changes in rainfall might be considered much rarer than they actually are [*Cohn and Lins*, 2005]. Lastly, it was shown as well, that the autocorrelation function significantly departs from the case of independence.

Although the above findings are in favour of the existence of a stronger dependence structure than the one typically assumed in literature [*Potter*, 1979; *Fraedrich and Blender*, 2003; *Kantelhardt et al.*, 2006], it seems that there is a discrepancy between smaller and larger time scales [*Fraedrich and Larnder*, 1993; *Pelletier and Turcotte*, 1997; *Poveda*, 2011; *Ault et al.*, 2013]. To this end, the most important source of uncertainty in the determination of LRD, which is the record length, should not be overlooked [*Koutsoyiannis*, 2002; *Koutsoyiannis and Montanari*, 2007]. Although using stations with relatively high —compared to the majority of the existing rainfall data records— record length, the accurate detection of long range dependence cannot be guaranteed because this behaviour may require even longer record length to be revealed. Subsequently, the low estimates of Hurst parameter in instrumental time series could be attributed to the limited record length available in some cases and therefore, should be considered characteristic only for this time horizon of approximately 100 years. This behaviour of LRD is illustrated in the case of paleoclimatic data with annual time-step; when the sample size of paleoclimatic data is restricted to match the one of instrumental data (approximately 100 years) the distribution of the estimated Hurst coefficient exhibits a lower mean value together with an increased variance, compared to the one arising from larger sample sizes. However, these results could not be reproduced for paleoclimatic series of longer time-scales, i.e. above decadal, which suggests that the discrepancy in LRD structure**,** i.e. the difference in the mean value of H between sub-decadal (annual as in the instrumental series) and above-decadal (as in the paleoclimatic series) scales, may be nonetheless inherent in precipitation behaviour, rather than being solely attributed to the sample size effect. This finding is in good agreement with a recently published work by Markonis and Koutsoyiannis [2016], which emphasizes the influence of time-scale when it comes to the analysis of the dependence of a time-series.

In addition, due to historical and socio-economic reasons, the data set does not include enough or any stations at all adequate for our analysis, from certain regions of the world such as Central Africa and South America. However, the representation of climates according to the Köppen classification system remains fairly good since a wide variety of climates is still represented in North America, Australia and Central Europe, i.e. the areas which contribute the most to our dataset. Even so, the possibility of a misrepresentation of climates cannot be excluded and this constitutes a source of uncertainty in our results and an area open for research in the future, when more stations of larger record lengths will be made publicly available.

It is also important to consider the uncertainty induced due to measurement errors or false homogenization techniques which may introduce bias to the estimation of LRD [Steirou, 2011]. GHCN-Daily highlights the potential bias provoked by changes in instrumentation over the years and it is possible that this kind of bias could also affect the estimation of H.

Ultimately, the high variability of the results is in accordance with the inherent uncertainty of the phenomenon, apart from algorithmic or data choices. An important conclusion drawn from the analysis is that simplifying assumptions commonly used in practice, such as inter-annual independence, may, in cases, significantly, depart from reality and hence, a thorough and careful study of the dependence properties of the dataset, as performed here, is recommended, especially when longer time horizons are of interest.

References

Akkemik, Ü., Dağdeviren, N., & Aras, A. (2005). A preliminary reconstruction (AD 1635–2000) of spring precipitation using oak tree rings in the western Black Sea region of Turkey. *International Journal of Biometeorology*, *49*(5), 297-302.

Asmerom, Y., Polyak, V., Burns, S., & Rassmussen, J. (2007). Solar forcing of Holocene climate: New insights from a speleothem record, southwestern United States. Geology, 35(1), 1-4.

Ault, T. R., J. E. Cole, J. T. Overpeck, G. T. Pederson, S. St. George, B. Otto-Bliesner, C. A. Woodhouse, and C. Deser (2013), The continuum of hydroclimate variability in western North America during the last millennium, Journal of Climate, 26(16), 5863-5878.

Bakke, J., Dahl, S. O., & Nesje, A. (2005). Lateglacial and early Holocene palaeoclimatic reconstruction based on glacier fluctuations and equilibrium-line altitudes at northern Folgefonna, Hardanger, western Norway. Journal of Quaternary Science, 20(2), 179-198.

Bale, R. J., Robertson, I., Salzer, M. W., Loader, N. J., Leavitt, S. W., Gagen, M., ... & McCarroll, D. (2011). An annually resolved bristlecone pine carbon isotope chronology for the last millennium. Quaternary Research, 76(1), 22-29.

Bar-Matthews, M., Ayalon, A., Gilmour, M., Matthews, A., & Hawkesworth, C. J. (2003). Sea–land oxygen isotopic relationships from planktonic foraminifera and speleothems in the Eastern Mediterranean region and their implication for paleorainfall during interglacial intervals. Geochimica et Cosmochimica Acta, 67(17), 3181-3199.

Beran, J. (1994), Statistics for long-memory processes, CRC Press.

Briffa, K. R., P. D. Jones, F. H. Schweingruber, W. Karlén, and S. G. Shiyatov (1996), Tree-ring variables as proxy-climate indicators: problems with low-frequency signals, in Climatic Variations and Forcing Mechanisms of the Last 2000 Years, edited, pp. 9-41, Springer.

Briffa, K. R., P. D. Jones, T. S. Bartholin, D. Eckstein, F. H. Schweingruber, W. Karlen, P. Zetterberg, and M. Eronen (1992), Fennoscandian summers from AD 500: temperature changes on short and long timescales, Climate dynamics, 7(3), 111-119.

Bunde, A., U. Büntgen, J. Ludescher, J. Luterbacher, and H. von Storch (2013), Is there memory in precipitation?, Nature Climate Change, 3(3), 174-175.

Büntgen, U., Tegel, W., Nicolussi, K., McCormick, M., Frank, D., Trouet, V., ... & Luterbacher, J. (2011). 2500 years of European climate variability and human susceptibility. Science, 331(6017), 578-582.

Cleaveland, M. K., Stahle, D. W., Therrell, M. D., Villanueva-Diaz, J., & Burns, B. T. (2003). Tree-ring reconstructed winter precipitation and tropical teleconnections in Durango, Mexico. Climatic Change, 59(3), 369-388.

Cohn, T. A., and H. F. Lins (2005), Nature's style: Naturally trendy, Geophysical Research Letters, 32(23).

Cooper, R. J., Melvin, T. M., Tyers, I., Wilson, R. J., & Briffa, K. R. (2013). A tree-ring reconstruction of East Anglian (UK) hydroclimate variability over the last millennium. Climate dynamics, 40(3-4), 1019-1039.

Dee, S., J. Emile-Geay, M. Evans, A. Allam, E. Steig, and D. Thompson (2015), PRYSM: An open-source framework for Proxy System Modeling, with applications to oxygen-isotope systems, Journal of Advances in Modeling Earth Systems, 7(3), 1220-1247.

Denniston, R. F., González, L. A., Baker, R. G., Asmerom, Y., Reagan, M. K., Edwards, R. L., & Alexander, E. C. (1999). Speleothem evidence for Holocene fluctuations of the prairie-forest ecotone, north-central USA. The Holocene, 9(6), 671-676.

Díaz, S. C., Therrell, M. D., Stahle, D. W., & Cleaveland, M. K. (2002). Chihuahua (Mexico) winter-spring precipitation reconstructed from tree-rings, 1647-1992. Climate Research, 22(3), 237-244.

Díaz, S. C., Touchan, R., & Swetnam, T. W. (2001). A tree-ring reconstruction of past precipitation for Baja California Sur, Mexico. International Journal of Climatology, 21(8), 1007-1019.

Dimitriadis, P., and D. Koutsoyiannis (2015), Climacogram versus autocovariance and power spectrum in stochastic modelling for Markovian and Hurst–Kolmogorov processes, Stochastic Environmental Research and Risk Assessment, 1-21.

Elbert, J., Grosjean, M., von Gunten, L., Urrutia, R., Fischer, D., Wartenburger, R., Ariztegui, D., and Fujak, M. (2012). Quantitative high-resolution winter (JJA) precipitation reconstruction from varved sediments of Lago Plomo 47 S, Patagonian Andes, AD 1530–2001, Holocene, 22, 465–474.

Faulstich, H. L., Woodhouse, C. A., & Griffin, D. (2013). Reconstructed cool-and warm-season precipitation over the tribal lands of northeastern Arizona. Climatic change, 118(2), 457-468.

Fleitmann, D., Cheng, H., Badertscher, S., Edwards, R. L., Mudelsee, M., Göktürk, O. M., ... & Kramers, J. (2009). Timing and climatic impact of Greenland interstadials recorded in stalagmites from northern Turkey. Geophysical Research Letters, 36(19).

Fraedrich, K., and C. Larnder (1993), Scaling regimes of composite rainfall time series, Tellus A, 45(4), 289-298.

Fraedrich, K., and R. Blender (2003), Scaling of atmosphere and ocean temperature correlations in observations and climate models, Physical Review Letters, 90(10), 108501.

Franke, J., D. Frank, C. C. Raible, J. Esper, and S. Brönnimann (2013), Spectral biases in tree-ring climate proxies, Nature Climate Change, 3(4), 360-364.

Granger, Clive WJ. (1980), Long memory relationships and the aggregation of dynamic models Journal of econometrics, 14.2: 227-238.

Griffin, D., & Anchukaitis, K. J. (2014). How unusual is the 2012–2014 California drought?. Geophysical Research Letters, 41(24), 9017-9023.

Griffin, D., Woodhouse, C. A., Meko, D. M., Stahle, D. W., Faulstich, H. L., Carrillo, C., ... & Leavitt, S. W. (2013). North American monsoon precipitation reconstructed from tree-ring latewood. Geophysical Research Letters, 40(5), 954-958.

Griffiths, M. L., Drysdale, R. N., Vonhof, H. B., Gagan, M. K., Zhao, J. X., Ayliffe, L. K., ... & Suwargadi, B. W. (2010). Younger Dryas–Holocene temperature and rainfall history of southern Indonesia from δ 18 O in speleothem calcite and fluid inclusions. Earth and Planetary Science Letters, 295(1), 30-36.

Griggs, C., DeGaetano, A., Kuniholm, P., & Newton, M. (2007). A regional high-frequency reconstruction of May–June precipitation in the north Aegean from oak tree rings, AD 1089–1989. International Journal of Climatology, 27(8), 1075-1089.

Grissino-Mayer, H. D., & Fritts, H. C. (1997). The International Tree-Ring Data Bank: an enhanced global database serving the global scientific community. The Holocene, 7(2), 235-238.

Haslett, J., and A. E. Raftery (1989), Space-time modelling with long-memory dependence: Assessing Ireland's wind power resource, Applied Statistics, 1-50.

Helama, S., M. Lindholm, M. Timonen, and M. Eronen (2004), Detection of climate signal in dendrochronological data analysis: a comparison of tree-ring standardization methods, Theoretical and Applied Climatology, 79(3-4), 239-254.

Holmgren, K., Karlén, W., Lauritzen, S. E., Lee-Thorp, J. A., Partridge, T. C., Piketh, S., ... & Tyson, P. D. (1999). A 3000-year high-resolution stalagmitebased record of palaeoclimate for northeastern South Africa. The Holocene, 9(3), 295-309.

Holmgren, K., Lee-Thorp, J. A., Cooper, G. R., Lundblad, K., Partridge, T. C., Scott, L., ... & Tyson, P. D. (2003). Persistent millennial-scale climatic variability over the past 25,000 years in Southern Africa. Quaternary Science Reviews, 22(21), 2311-2326.

Hu, C., Henderson, G. M., Huang, J., Xie, S., Sun, Y., & Johnson, K. R. (2008). Quantification of Holocene Asian monsoon rainfall from spatially separated cave records. Earth and Planetary Science Letters, 266(3), 221-232.

Hurst, H. E. (1951), Long-term storage capacity of reservoirs, Trans. Amer. Soc. Civil Eng., 116, 770-808.

Kantelhardt, J. W., E. Koscielny-Bunde, D. Rybski, P. Braun, A. Bunde, and S. Havlin (2006), Long-term persistence and multifractality of precipitation and river runoff records, Journal of Geophysical Research: Atmospheres (1984–2012), 111(D1).

Koutsoyiannis, D. (2002), The Hurst phenomenon and fractional Gaussian noise made easy, Hydrological Sciences Journal, 47(4), 573-595.

Koutsoyiannis, D. (2003), Climate change, the Hurst phenomenon, and hydrological statistics, Hydrological Sciences Journal, 48(1), 3-24.

Koutsoyiannis, D. (2011a), Hurst–Kolmogorov dynamics as a result of extremal entropy production, Physica A: Statistical Mechanics and its Applications, 390(8), 1424-1432.

Koutsoyiannis, D. (2011b), Hurst-Kolmogorov Dynamics and Uncertainty, JAWRA Journal of the American Water Resources Association, 47(3), 481-495.

Koutsoyiannis, D., and A. Montanari (2007), Statistical analysis of hydroclimatic time series: Uncertainty and insights, Water Resources Research, 43(5).

Lough, J. M. (2007). Tropical river flow and rainfall reconstructions from coral luminescence: Great Barrier Reef, Australia, Paleoceanography, PA2218, doi:10.1029/2006PA00137

Malevich, S. B., Woodhouse, C. A., & Meko, D. M. (2013). Tree-ring reconstructed hydroclimate of the Upper Klamath basin. Journal of Hydrology, 495, 13-22.

Mandelbrot, B., and J. Wallis (1969), Some long-run properties of geophysical records, Water resources research, 5(2), 321-340.

Markonis Y. and D. Koutsoyiannis, (2016), Scale-dependence of persistence in precipitation records, Nature Climate Change, 6 (4), 399-401.

Markonis, Y. (2015), Stochastic Investigation of Large-Scale Hydroclimatic Correlations over the Mediterranean, PhD Thesis.

Markonis, Y., and D. Koutsoyiannis (2013), Climatic variability over time scales spanning nine orders of magnitude: Connecting Milankovitch cycles with Hurst–Kolmogorov dynamics, Surveys in Geophysics, 34(2), 181-207.

Ni, F., T. Cavazos, M. K. Hughes, A. C. Comrie, and G. Funkhouser (2002), Cool-season precipitation in the southwestern USA since AD 1000: comparison of linear and nonlinear techniques for reconstruction, International Journal of Climatology, 22(13), 1645-1662.

O’Connell, E., D. Koutsoyiannis, H. F. Lins, Y. Markonis, A. Montanari, and T. Cohn (2015),The scientific legacy of Harold Edwin Hurst (1880 – 1978), Hydrological Sciences Journal, Special issue: Facets of Uncertainty, 2015, doi: 10.1080/02626667.2015.1125998.

Papalexiou, S. M., and D. Koutsoyiannis (2012), Entropy based derivation of probability distributions: A case study to daily rainfall, Advances in Water Resources, 45, 51-57.

Papalexiou, S. M., D. Koutsoyiannis, and A. Montanari (2011), Can a simple stochastic model generate rich patterns of rainfall events?, Journal of hydrology, 411(3), 279-289.

Pederson, N., Jacoby, G. C., D'Arrigo, R. D., Cook, E. R., Buckley, B. M., Dugarjav, C., & Mijiddorj, R. (2001). Hydrometeorological reconstructions for Northeastern Mongolia derived from tree rings: 1651-1995*. Journal of Climate, 14(5), 872-881.

Pelletier, J. D. (1998), The power spectral density of atmospheric temperature from time scales of 10− 2 to 10 6 yr, Earth and planetary science letters, 158(3), 157-164.

Pelletier, J. D., and D. L. Turcotte (1997), Long-range persistence in climatological and hydrological time series: analysis, modeling and application to drought hazard assessment, Journal of Hydrology, 203(1), 198-208.

Potter, K. W. (1979), Annual precipitation in the northeast United States: Long memory, short memory, or no memory?, Water Resources Research, 15(2), 340-346.

Poveda, G. (2011), Mixed memory,(non) Hurst effect, and maximum entropy of rainfall in the tropical Andes, Advances in Water Resources, 34(2), 243-256.

Romero-Viana, L., Julià, R., Schimmel, M., Camacho, A., Vicente, E., & Miracle, M. R. (2011). Reconstruction of annual winter rainfall since AD 1579 in central-eastern Spain based on calcite laminated sediment from Lake La Cruz. Climatic change, 107(3-4), 343-361.

Salzer, M. W., & Kipfmueller, K. F. (2005). Reconstructed temperature and precipitation on a millennial timescale from tree-rings in the southern Colorado Plateau, USA. Climatic Change, 70(3), 465-487.

Saunders, K.M., Kamenik, C., Hodgson, D.A., Hunziker, S., Siffert, L., Fischer, D., Fujak, M., Gibson, J.A.E., Grosjean, M., (2012). Late Holocene changes in precipitation in northwest Tasmania and their potential links to shifts in the Southern Hemisphere westerly winds. Global and Planetary Change 92, 82-91.

Springer, G. S., Rowe, H. D., Hardt, B., Edwards, R. L., & Cheng, H. (2008). Solar forcing of Holocene droughts in a stalagmite record from West Virginia in east-central North America. Geophysical Research Letters, 35(17).

St George, S., & Nielsen, E. (2002). Flood ring evidence and its application to paleoflood hydrology of the Red River and Assiniboine River in Manitoba. Geographie physique et Quaternaire, 56(2-3), 181-190.

Steinman BA, Abbott MB, Mann ME, Stansell ND, Finney BP. (2012). 1,500 year quantitative reconstruction of winter precipitation in the Pacific Northwest. Proceedings of the National Academy of Sciences of the United States of America. 109(29):11619-11623. doi:10.1073/pnas.1201083109.

Steirou, E. (2011), Investigation of methods for hydroclimatic data homogenization, National Technical University of Athens, Athens.

Stephenson, D. B., V. Pavan, and R. Bojariu (2000), Is the North Atlantic Oscillation a random walk?, International Journal of Climatology, 20(1), 1-18.

Tan, L., Cai, Y., An, Z., Edwards, R. L., Cheng, H., Shen, C.-C., and Zhang, H. (2011). Centennial- to decadal-scale monsoon precipitation variability in the semi-humid region, northern China during the last 1860 years: Records from stalagmites in Huangye Cave, Holocene, 21, 287–296.

Touchan, R., Funkhouser, G., Hughes, M. K., & Erkan, N. (2005). Standardized precipitation index reconstructed from Turkish tree-ring widths. Climatic Change, 72(3), 339-353.

Touchan, R., Meko, D., & Hughes, M. K. (1999). A 396-YEAR RECONSTRUCTION OF PRECIPITATION IN SOUTHERN JORDAN1. JAWRA Journal of the American Water Resources Association, 35(1), 49-59.

Tyralis, H., and D. Koutsoyiannis (2011), Simultaneous estimation of the parameters of the Hurst–Kolmogorov stochastic process, Stochastic Environmental Research and Risk Assessment, 25(1), 21-33.

Van Breukelen, M. R., Vonhof, H. B., Hellstrom, J. C., Wester, W. C. G., & Kroon, D. (2008). Fossil dripwater in stalagmites reveals Holocene temperature and rainfall variation in Amazonia. Earth and Planetary Science Letters, 275(1), 54-60.

Viau, A. E., & Gajewski, K. (2009). Reconstructing millennial-scale, regional paleoclimates of boreal Canada during the Holocene. Journal of Climate, 22(2), 316-330.

Viau, A. E., Gajewski, K., Sawada, M. C., & Bunbury, J. (2008). Low-and high-frequency climate variability in eastern Beringia during the past 25 000 years. Canadian Journal of Earth Sciences, 45(11), 1435-1453.

Wang, Y., Cheng, H., Edwards, R. L., He, Y., Kong, X., An, Z., ... & Li, X. (2005). The Holocene Asian monsoon: links to solar changes and North Atlantic climate. Science, 308(5723), 854-857.

Williams, P. W., Neil, H. L., & Zhao, J. X. (2010). Age frequency distribution and revised stable isotope curves for New Zealand speleothems: palaeoclimatic implications. International Journal of Speleology, 39(2), 5.

Wilson, R., Loader, N. J., Rydval, M., Patton, H., Frith, A., Mills, C. M., ... & Gunnarson, B. E. (2012). Reconstructing Holocene climate from tree rings: The potential for a long chronology from the Scottish Highlands. The Holocene, 22(1), 3-11.

Yang, B., Qin, C., Wang, J., He, M., Melvin, T. M., Osborn, T. J., & Briffa, K. R. (2014). A 3,500-year tree-ring record of annual precipitation on the northeastern Tibetan Plateau. Proceedings of the National Academy of Sciences, 111(8), 2903-2908.

Yuan, D., Cheng, H., Edwards, R. L., Dykoski, C. A., Kelly, M. J., Zhang, M., ... & Dorale, J. A. (2004). Timing, duration, and transitions of the last interglacial Asian monsoon. Science, 304(5670), 575-578.

Zhai, Y., Y. Guo, J. Zhou, N. Guo, J. Wang, and Y. Teng (2014), The spatio-temporal variability of annual precipitation and its local impact factors during 1724–2010 in Beijing, China, Hydrological Processes, 28(4), 2192-2201.

Tables

Table 1 Rainfall reconstructions properties. *Area* presents the area covered by the reconstruction in thousand km^2; *Start* and *End* refer to years, in absolute chronology for tree rings and years before present (1950) for the other two data sets; and *Res* refers to time resolution in years.

Tree-rings									
Site	Location	Lat	Lon	Area	Start	End	Size	Res	Reference
CL02	Arizona, N. Mexico; USA	34°-38°N	105°-120°W	739.3	1000	1988	988	1	Ni et al. 2002
Kl13	Klameth; California, Oregon; USA	37°-44°N	119°-123°W	345	1000 & 1610	2004 & 2010	1004 & 406	1	Malevich et al. 2013
Du03	Durango; Mexico	24°-26°N	104°-105°W	24.6	1386	1993	607	1	Cleaveland et al. 2003
EA13	East Anglia; UK	52°-53°N	0°-2°E	24.6	900	2009	1109	1	Cooper et al. 2013
Ma02	Manitoba; Canada	49°-50°N	96°-97°W	12.3	1409	1998	589	1	St. George et al. 2002
Mo01	NE Mongolia	48°-49°N	107°-110°E	86.2	1651	1995	344	1	Pederson et al. 2001
BC01	Baja California; Mexico	23°N	110°W	-	1571	1977	406	1	Díaz et al. 2001
Ca14	California; USA	34°-36°N	118°-121°W	73.9	1293	2014	721	1	Griffin et al. 2014
Ch02	Chihuahua; Mexico	26°-31°N	104°-109°W	308	1667	1992	325	1	Díaz et al. 2002
Ar12	NE Arizona, USA	36°-38°N	108°-110°W	49.3	1349	2008	659	1	Faulstich et al. 2013
NA07	North Aegean; Greece & Turkey	39°-42°N	22°-37°E	554.4	1089	1989	900	1	Griggs et al. 2007
RG97	Rio Grande; New Mexico; USA	29°-34°N	105°-108°W	184.8	622	1994	1372	1	Grissino-Mayer H. et al. 1997
SE12	South-central England	51°-53°N	0°-3°W	73.9	950	2009	1059	1	Wilson et al. 2012
Ti14	Tibet; China	37°-39°N	97°-100°E	73.9	-1500	2011	3511	1	Yang B et al. 2014
WM11	White Mountains; California; USA	37°N	118°W	-	1085	2005	920	1	Bale et al. 2011
Co05	Colorado; Arizona; USA	36°-37°N	110°-111°	12.3	570	1987	1417	1	Salzer et al. 2005
CE11	Central Europe	40°-50°N	2°-15°E	1602	-398	2008	2406	1	Büntgen et al. 2011
SJ99	South Jordan	30°N	36°E	-	1600	1995	395	1	Touchan et al. 1999
BS05	Black Sea; Turkey	41°-42°N	32°-34°E	24.6	1635	2000	365	1	Akkemik et al. 2005
Tu01	Turkey		*Unavailable*		1628	1980	305	1	
ST05	Southern Turkey	37°-38°N	31°-34°E	<0.1	1689	1994	305	1	Akkemik et al. 2005
NA13	North America; USA	30°-35°N	108°-113°W	<0.1	1530	2008	478	1	Griffin et al. 2013
EM05	Eastern Mediterranean	35°-40°N	20°-40°E	1100	1400	2000	600	1	Touchan et al. 2005

Site	Location	Lat	Lon	Area	Start	End	Size	Res	Reference
BCC-002	Buckeye Creek Cave; West Virginia; USA	38°N	80°W	-	67	6937	230	30	Springer et al. 2008
T7	Cold Air Cave; South Africa	24°S	29°E	-	-36	6404	645	10	Holmgren et al. 1999
T8	Cold Air Cave; South Africa	24°S	29°E	-	-41	7925	1139	7	Holmgren et al. 2003
CWC-1s	Cold Water Cave; Iowa; USA	43°N	92°W	-	10	7760	156	50	Denniston et al. 1999
CWC-3L	Cold Water Cave; Iowa; USA	43°N	92°W	-	2017	7857	147	40	Denniston et al. 1999
D4	Dongge Cave; China	25°N	108°E	-	14	7874	263	30	Yuan et al. 2004
DA	Dongge Cave; China	25°N	108°E	-	-47	7936	2662	3	Wang et al. 2005
HS-4	Heshang Cave; China	30°N	110°E	-	-42	7928	398	20	Hu et al. 2008
LR06-B1	Liang Luar Cave; Indonesia	9°S	120°E	-	-45	6444	928	7	Griffiths et al. 2010
LR06-B3	Liang Luar Cave; Indonesia	9°S	120°E	-	11	7861	158	50	Griffiths et al. 2010
A1	Lianhua Cave; China	29°N	110°E	-	-50	6586	1107	6	Cosford et al. 2009
NZ-1	South Island; New Zealand	42°S	172°E	-	568	7768	121	60	Williams et al. 2010
PP-1	Pink Panther Cave; New Mexico; USA	32°N	105°W	-	5	7905	396	20	Asmerom et al. 2007
So-1	Sofular Cave; Turkey	41°N	32°E	-	-52	7936	1998	4	Fleitmann et al. 2009
SCC-1	Soreq Cave; Israel	31°N	35°E	-	70	7910	113	70	Bar-Matthews et al. 2003
NC-A	Cueva del Tigre Perdido; Peru	6°S	77°W	-	44	4284	213	20	Van Breukelen et al. 2008

Site	Location	Lat	Lon	Area	Start	End	Size	Res	Reference
As05	Lake Aspvatnet; Norway	70°N	20°E	-	0	8000	80	100	Bakke et al. et al. 2005
Be08	Beringia; USA	60°-69°N	126°-166°W	4436	0	25000	250	100	Viau et al. 2008
CC09	Central Boreal; Canada	50°-70°N	80°-120°W	9857	0	11900	119	100	Viau et al. 2009
LC09	Labrador; Canada	50°-70°N	50°-65°W	3696	0	11900	119	100	Viau et al. 2009
LC11	La Cruz; Spain	40°N	2°W	-	1	371	370	1	Romero-Viana et al. 2011
LP12	Lago Plomo; Chile	47°S	73°W	-	-52	420	472	1	Elbert et al. 2012
MC09	MacKenzie; Canada	50°-70°N	120°-140°W	4928	0	11800	118	100	Viau et al. 2009
NC11	North central China	33°-42°N	104°-121°E	1885	-25	1755	178	10	L. Tan et al. 2011
QC09	Quebec; Canada	50°-70°N	65°-80°W	6161	0	9000	90	100	Viau et al. 2009
Qu07	Queensland; Australia	17°-23°S	147°-151°E	295.7	1631	1983	352	1	Lough et al. 2007
Sa12	Rebecca Lagoon; Tasmania; Australia	41°S	145°E	-	469	3654	637	5	Saunders et al. 2012
St12	Castor & Lime Lakes; USA	49°N	120°W	-	-52	1448	300	5	Steinman et al. 2012

Table 2 Summary statistics of the Hurst parameter as estimated from the aggregated variance method applied to the 1265 records. Q indicates the empirical quantile.

Min	$Q_{2.5}$	Q_{25}	Median	Q_{75}	$Q_{97.5}$	Max	Mean	SD
0.23	0.40	0.53	0.59	0.65	0.80	0.99	0.59	0.1

Table 3 Summary statistics of the Hurst parameter as estimated from the aggregated variance method and the LSSD method both applied to the 558 records without missing values. Q indicates the empirical quantile.

	Agg. var. method	LSSD method
Mean	0.56	0.58
SD	0.10	0.09
Min	0.28	0.33
$Q_{2.5}$	0.37	0.40
Q_{25}	0.50	0.52
Median	0.56	0.57
Q_{75}	0.63	0.64
$Q_{97.5}$	0.78	0.79
Max	0.90	0.92

Table 4 Summary statistics of the estimated autocorrelation coefficients for lags 1, 2, 3. Q indicates the empirical quantile.

	ρ_1	ρ_2	ρ_3
Mean	0.12	0.03	0.05
SD	0.11	0.12	0.11
Min	−0.19	−0.35	-0.32
$Q_{2.5}$	−0.10	−0.16	-0.15
Q_{25}	0.05	−0.05	-0.02
Median	0.11	0.02	0.05
Q_{75}	0.18	0.10	0.12
$Q_{97.5}$	0.37	0.29	0.27
Max	0.62	0.59	0.47

Figures

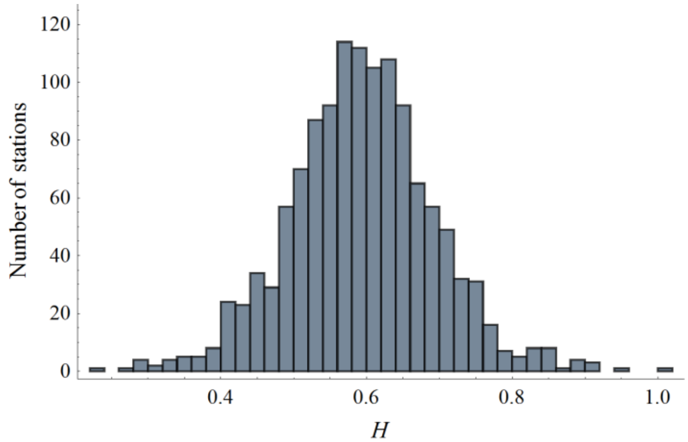

Figure 1 Empirical distribution of the Hurst coefficient *H* as obtained by applying the aggregated variance method to the 1265 annual rainfall records.

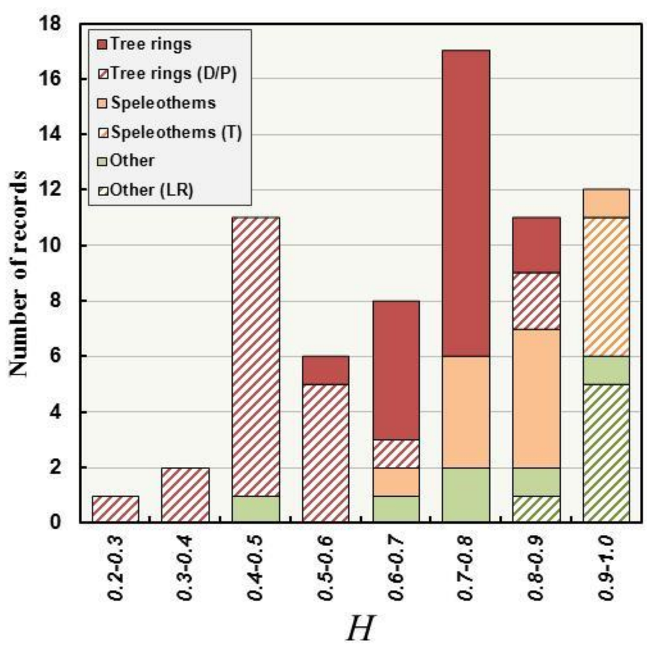

Figure 2 Empirical distribution of the Hurst coefficient *H* as obtained by applying the aggregated variance method to the paleoclimatic records. *Tree rings (D/P)* represents the detrended/pre-whitened time series; *Speleothems (T)* for time series exhibiting strong trends; *Other (LR)* for low resolution, 100-year-scale reconstructions (see Discussion).

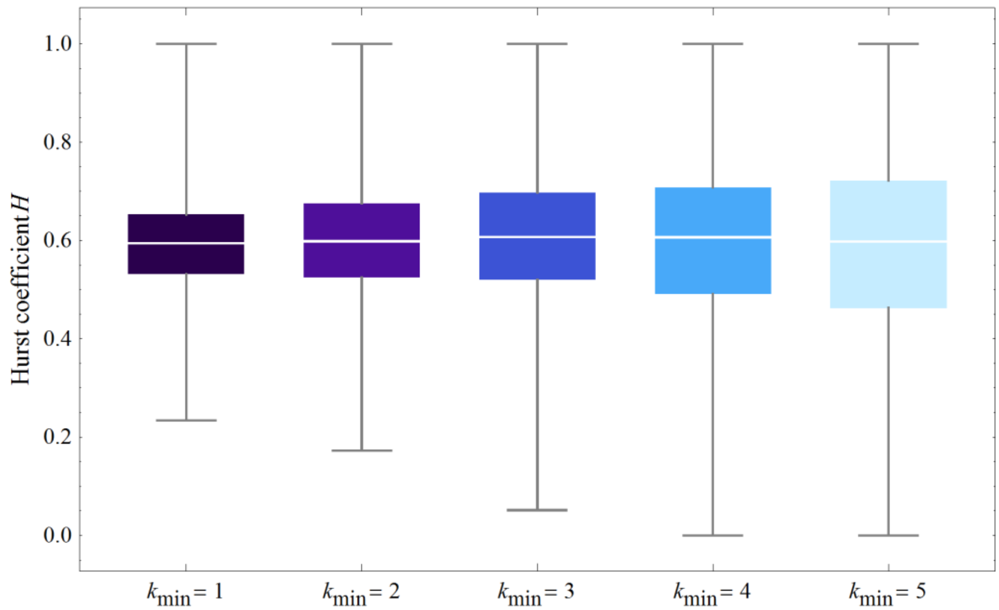

Figure 3 Box-plots depicting the sample differences resulting from variations in the value of minimum scale $k_{\min}$ when applying the aggregated variance method.

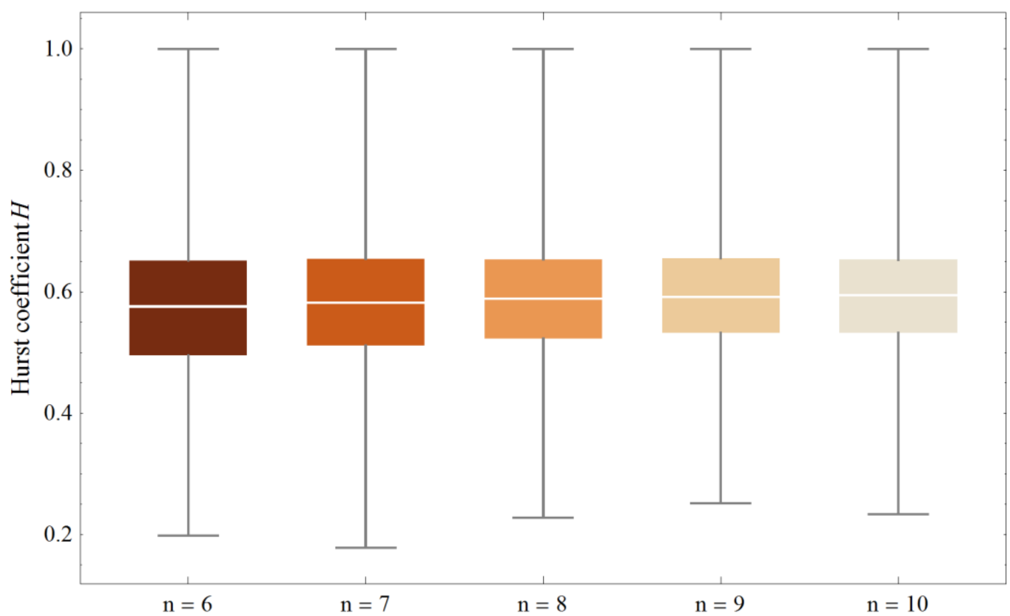

Figure 4 Box-plots depicting the sample differences resulting from variations in the number of minimum values n in $k_{\max}$ when applying the aggregated variance method.

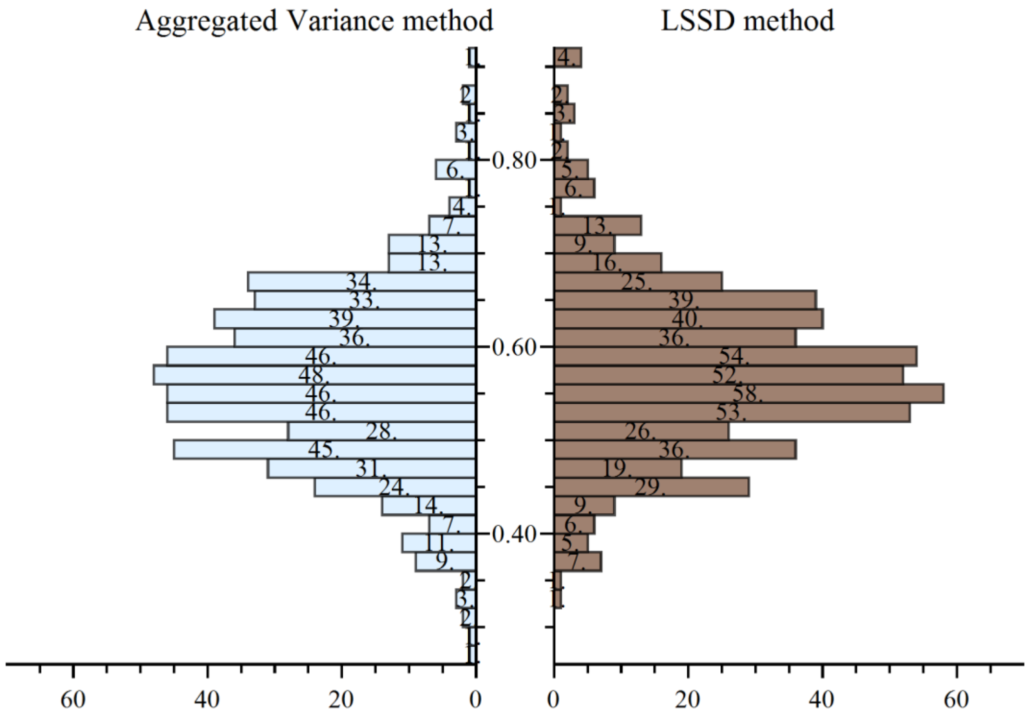

Figure 5 Double histogram depicting the empirical distribution of the Hurst coefficient *H* resulting from the aggregated variance method (left) and from the LSSD method (right), both applied to the 558 annual rainfall records without missing values.

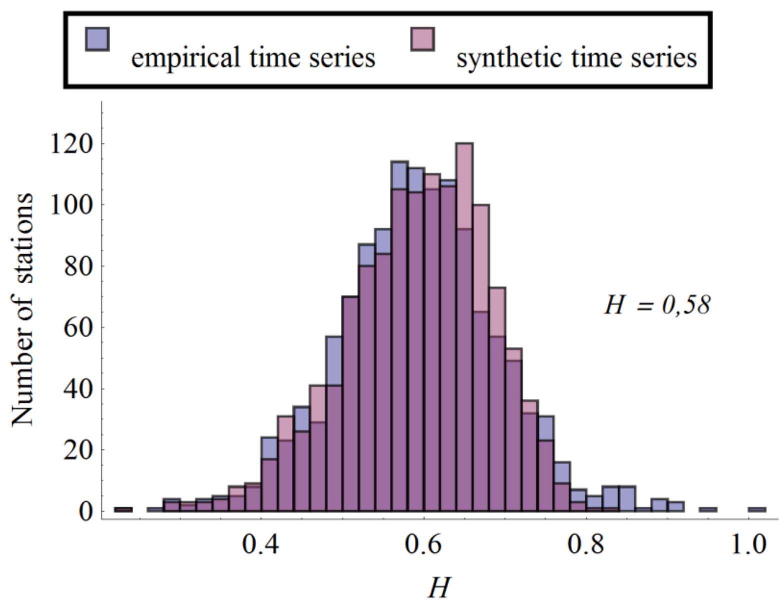

Figure 6 Paired histogram depicting the match of the empirical (blue) and theoretical (purple) distribution of the Hurst coefficient *H* resulting from applying the aggregated variance method to the 1265 historical records and 1265 synthetic records respectively. The synthetic records are realizations of a stochastic process characterized by a theoretical Hurst coefficient $H = 0.58$.

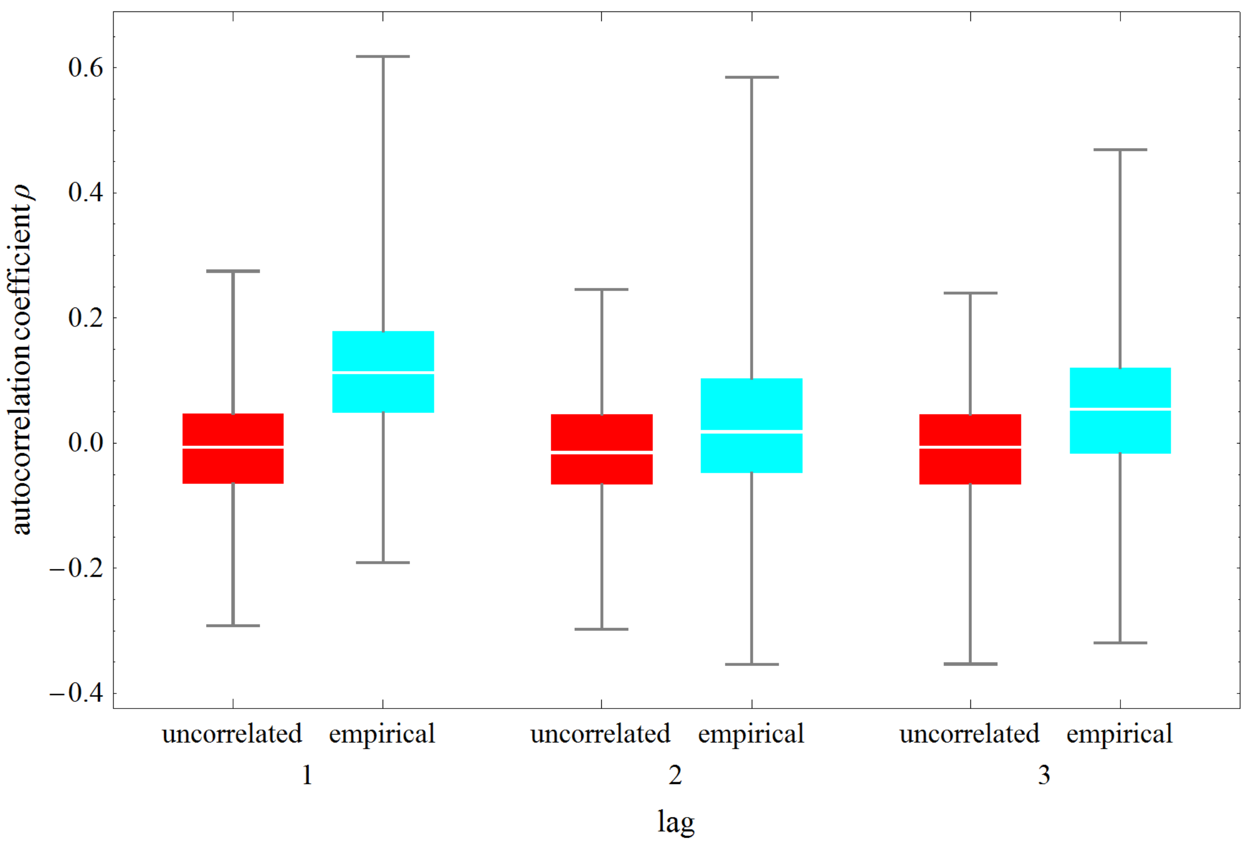

Figure 7 Box-plots depicting the resulting sample differences of the autocorrelation coefficient ρ between the empirical series and uncorrelated series for lags 1, 2, 3.

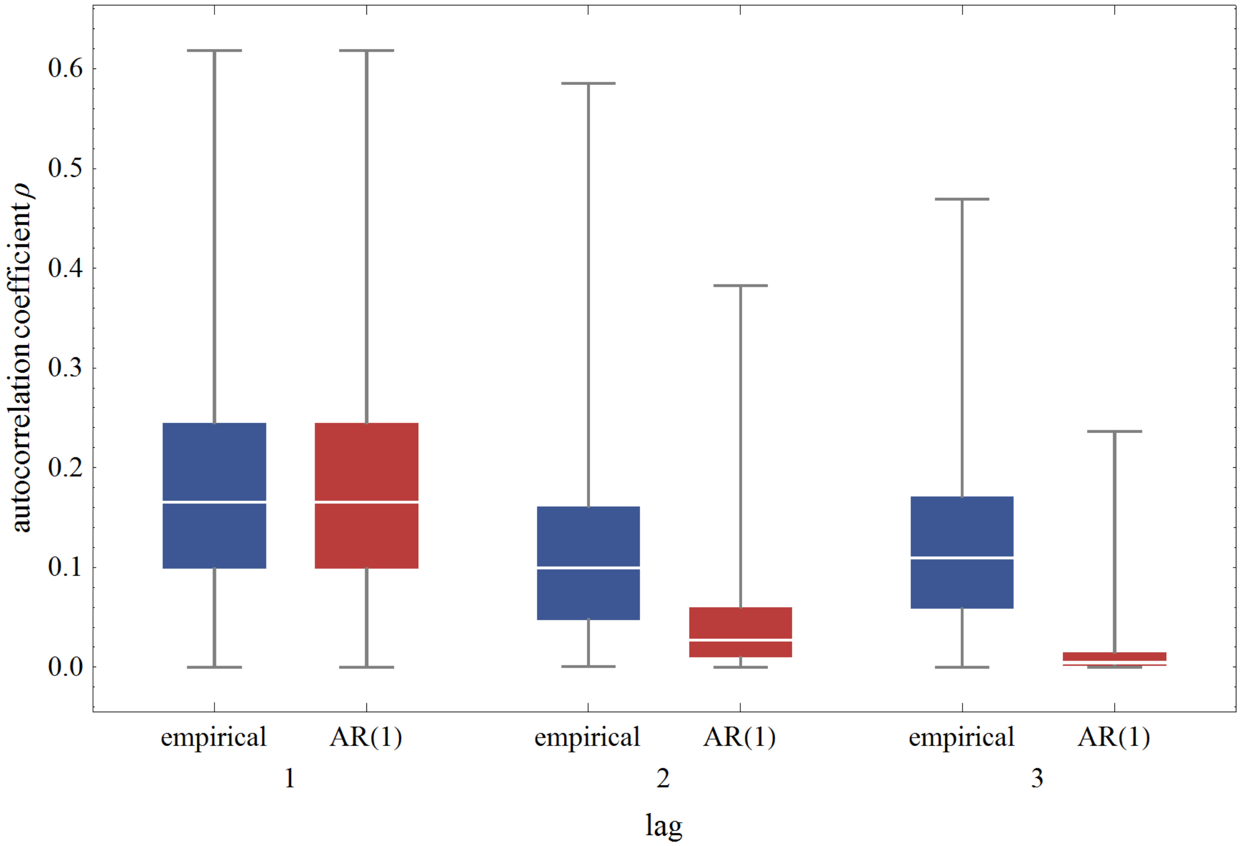

Figure 8 Box-plots showing the differences in the value of the autocorrelation coefficient ρ between the empirical estimates and the theoretical ones derived from an AR(1) model for lags 1, 2, 3.

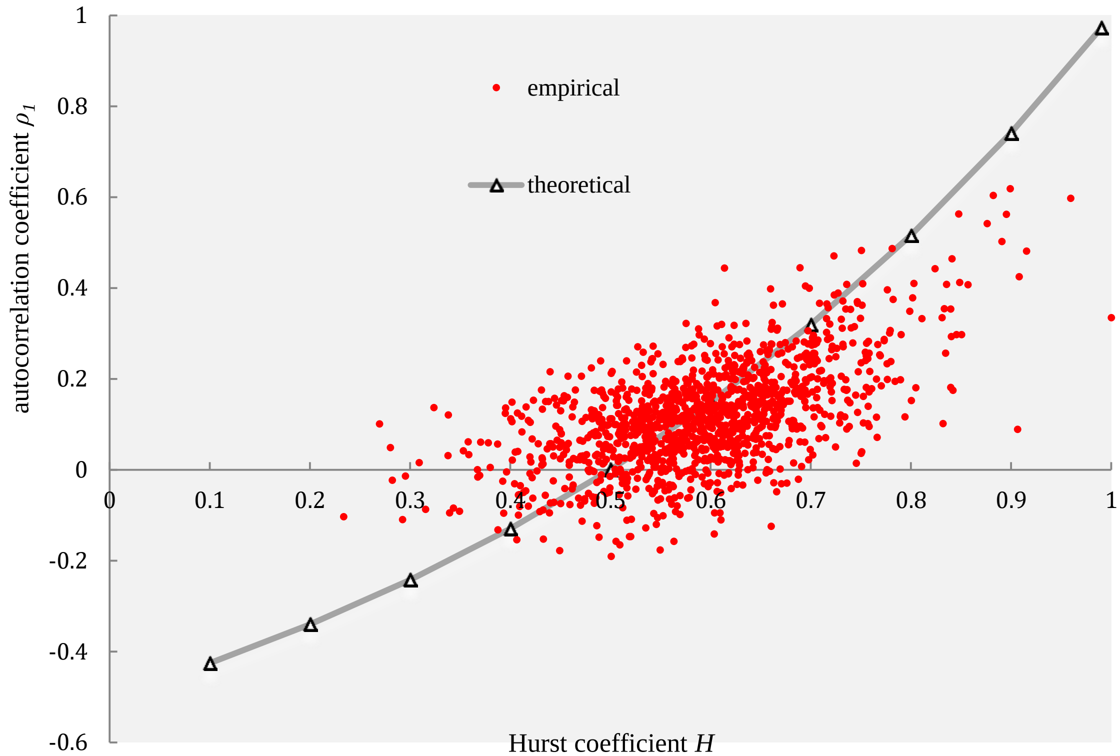

Figure 9 Empirical autocorrelation coefficient ρ_1 vs empirical Hurst coefficient H of the 1265 annual rainfall records and the theoretical line derived from a FGN model (Equation 3).

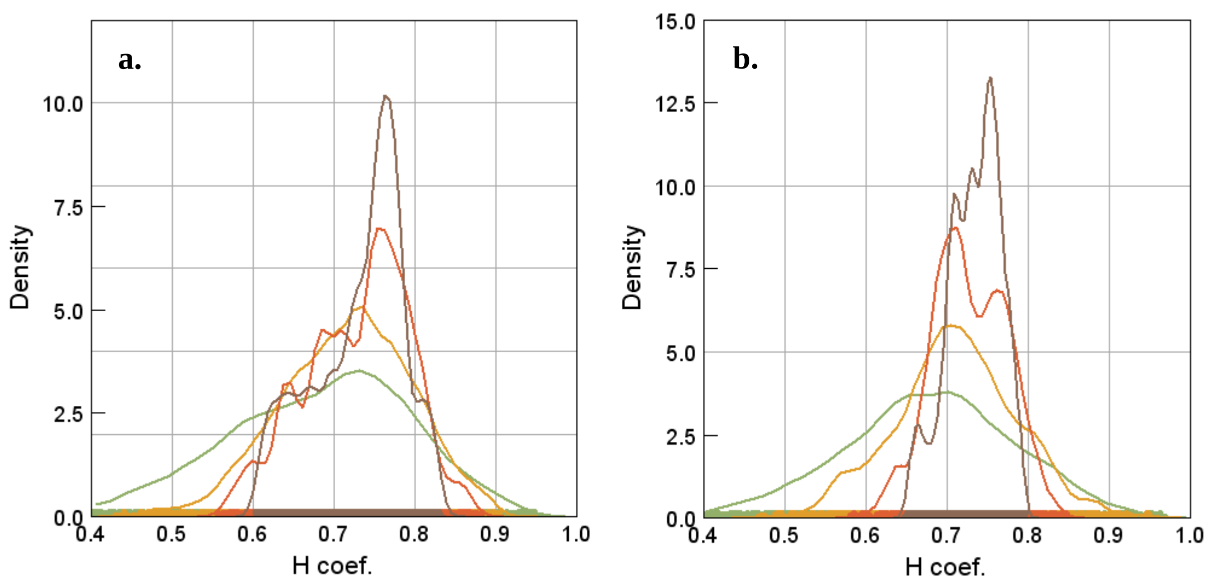

Figure 10 Empirical distributions of H estimation for different record lengths; *green* 50 years, *light orange* 100 years, *dark orange* 250 years, *brown* 500 years. **a.** CL02 dataset (15 records). **b.** Synthetic time series (H = 0.75, n = 15 records, L = 1000 years)